Supplementary Materials

Enhanced hydrogen evolution reaction performance of manganese-doped vanadium disulfide nanosheet across full ph spectrum and in simulated seawater

Ruonan Wang[1,2,#], Li Wan[1,#], Xinzheng Liu[1], Lixin Cao[1], Bohua Dong[1,*]

[1]School of Materials Science and Engineering, Ocean University of China,
1299 Sansha Road, Qingdao 266400, Shandong, China.
[2]Department of Mechanical and Electrical Engineering, Jining Polytechnic, No. 77, Jinyu Road, Jining 272000, Shandong, China.
[#]Authors contributed equally.

[*]**Correspondence to:** Prof. Bohua Dong, School of Materials Science and Engineering, Ocean University of China, Qingdao 266400, Shandong, China. E-mail: dongbohua@ouc.edu.cn

Experimental details

Materials

Oleylamine(15 Ω sq^{-1}), $VO(acac)_2$(99.99%), $MnCl_2$(99.99%), Pt/C(99.0%) were purchased from aladdin. Carbon cloth was purchased from CeTech. All chemicals were used as purchased without further purification.

Synthesis of VS_2

Sulfur powder (0.1 mmol) was dissolved in 5 mL of oleylamine and heated to 60°C under stirring. Simultaneously, 0.5 mmol of $VO(acac)_2$ was dissolved in 20 mL of oleylamine and stirred until homogeneous. The resulting solution was transferred to a 100 mL three-necked flask and heated to 140°C under a nitrogen atmosphere for 1 h. The sulfur solution in oleylamine was then injected into the flask, and the temperature was rapidly increased to 330°C and maintained for 1.5 h. After the reaction was complete and cooled to room temperature, the resultant product was collected by centrifugation and washed several times with cyclohexane and ethanol. The powder product was dried overnight at 60°C in an oven. Finally, the obtained powder was placed in a tube furnace and heated to 500°C under a nitrogen atmosphere for 1 h.

Synthesis of Mn-VS_2

The procedure was identical to that used for VS_2, with the addition of varying amounts of $MnCl_2$ to the $VO(acac)_2$ solution.

Synthesis of Mn-VS_2-Ox

The synthesis procedure was the same as for Mn-VS_2. After drying, the powder was calcined in air at 500°C for either 5 min or 60 min, resulting in Mn-VS_2-Ox-5 and Mn-VS_2-Ox-60, respectively.

Electrochemical Performance

A 1×1 cm^2 piece of carbon cloth was first ultrasonically cleaned in acetone for 15 min, then in ethanol for another 15 min, and finally in deionized water for 30 min to ensure thorough cleanliness. The cleaned carbon cloth was then used as the substrate electrode. A catalyst ink was prepared by ultrasonically dispersing 5.0 mg of the catalyst with 0.49 mL of anhydrous ethanol, 0.49 mL of deionized water, and 0.02 mL of 5 wt% Nafion solution for 30 minutes. Subsequently, 0.05 mL of this dispersion was uniformly coated on a 1×1 cm^2 area of the carbon cloth. The coated electrode was air-dried under vacuum conditions for use in electrochemical testing.

Electrochemical Measurements

All electrochemical tests were conducted using a CHI760E electrochemical workstation (Shanghai Chenhua Instruments, China) in a standard three-electrode system. The catalyst-loaded carbon cloth, with a catalyst loading of 0.25 mg and a working area of 1×1 cm^2, served as the working electrode. A carbon rod and an Ag/AgCl (saturated KCl) electrode were used as the counter and reference electrodes, respectively. The potentials measured were converted to values relative to the reversible hydrogen electrode (RHE) using the equation:

$$E_{(RHE)} = E_{(Ag/AgCl)} + 0.197 + 0.0591 \times pH$$

Due to the resistance at the catalyst-electrolyte interface, 95% iR compensation was applied. All electrochemical polarization tests were performed at a scan rate of 5 mV s^{-1}, and Tafel slopes were calculated using the Tafel equation:

$$\eta = b \times \log j + a$$

where η is the overpotential, b is the Tafel slope, j is the current density, and a is a constant. Electrochemical impedance spectroscopy (EIS) measurements were conducted in 0.5 M H_2SO_4 at overpotentials corresponding to 10 mA cm^{-2}, over frequencies ranging from 10 kHz to 0.1 Hz. Cyclic voltammetry (CV) tests were performed at scan rates ranging from 10 to 100 mV s^{-1} to calculate the double-layer capacitance (C_{dl}).

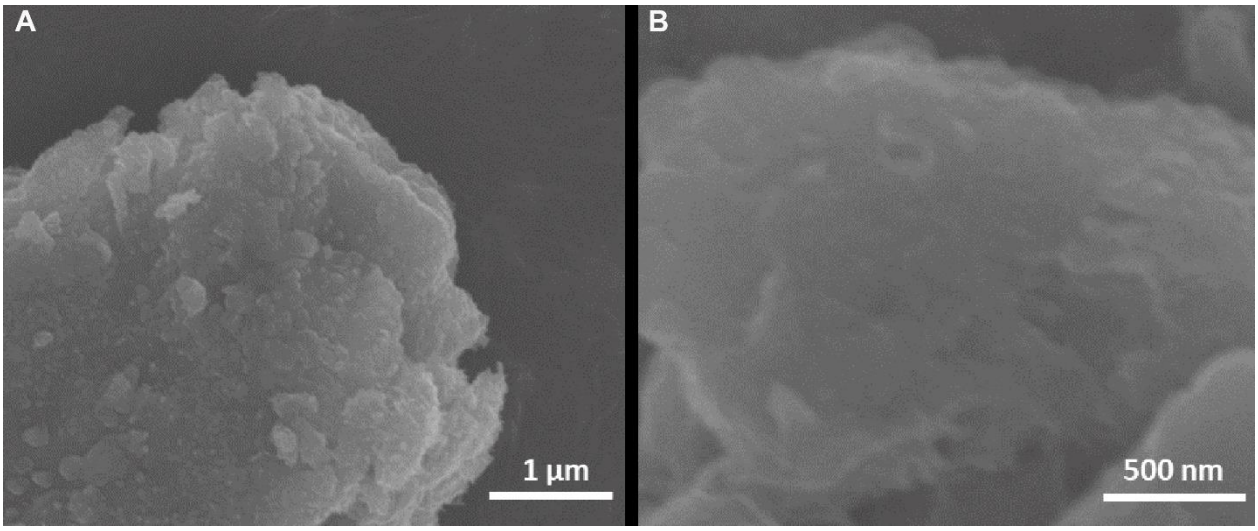

Supplementary Figure 1. SEM images of Mn-VS_2. As shown in (A and B), the as-synthesized Mn-VS2 exhibits a sheet-like morphology, evident from the SEM images taken at different magnifications. SEM: Scanning electron microscopy.

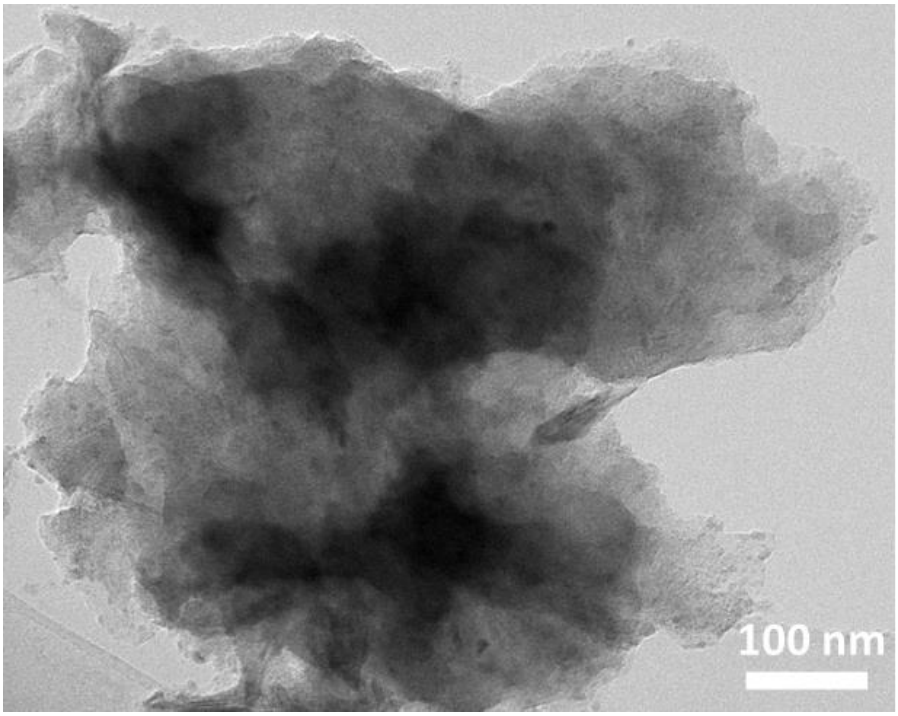

Supplementary Figure 2. TEM image of Mn-VS_2.

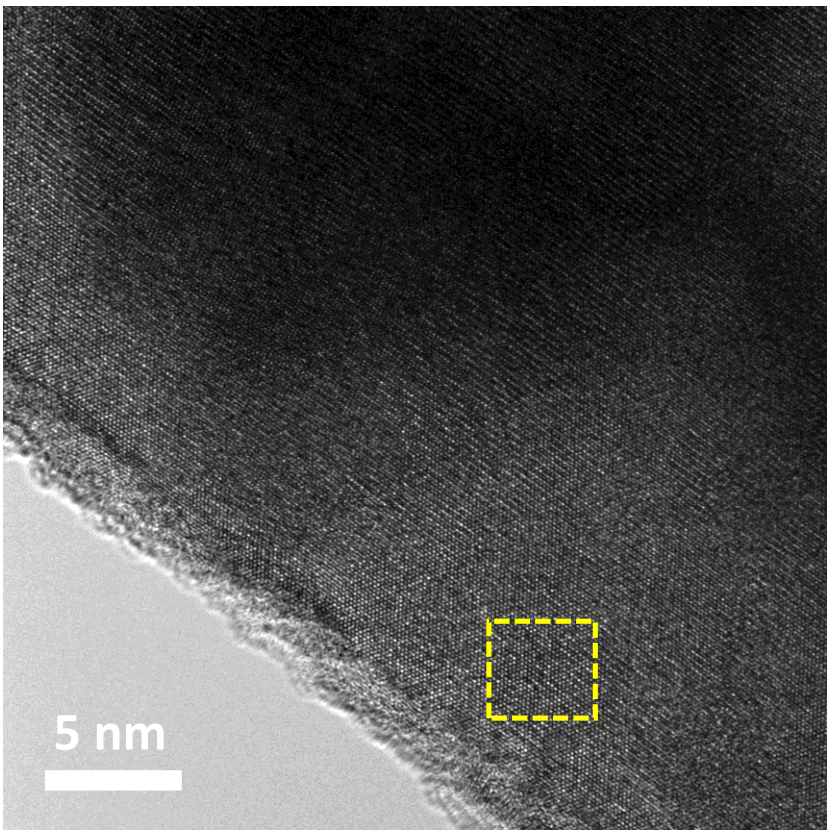

Supplementary Figure 3. HRTEM image of Mn-VS_2.

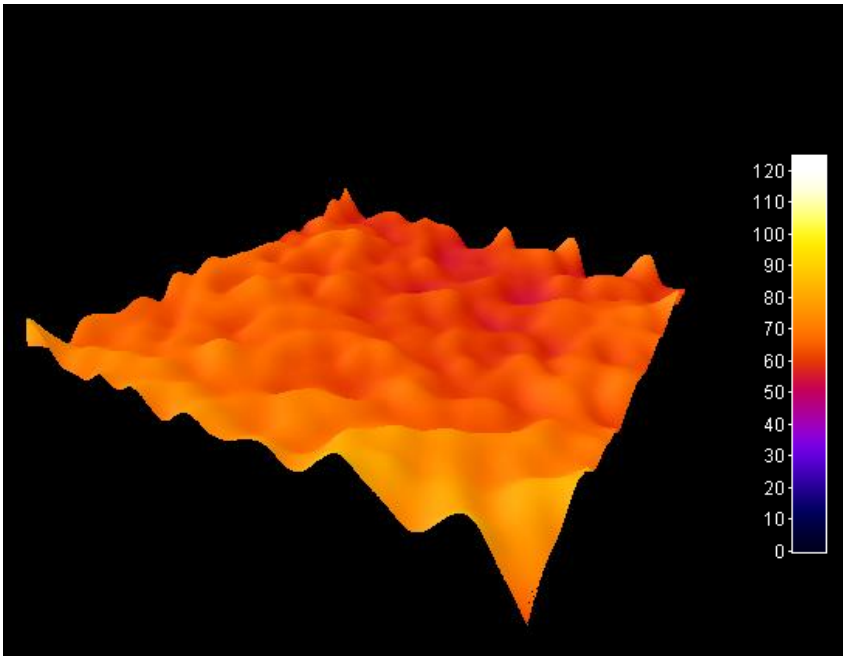

Supplementary Figure 4. 3D AOGF mappings from Supplementary Figure 1.

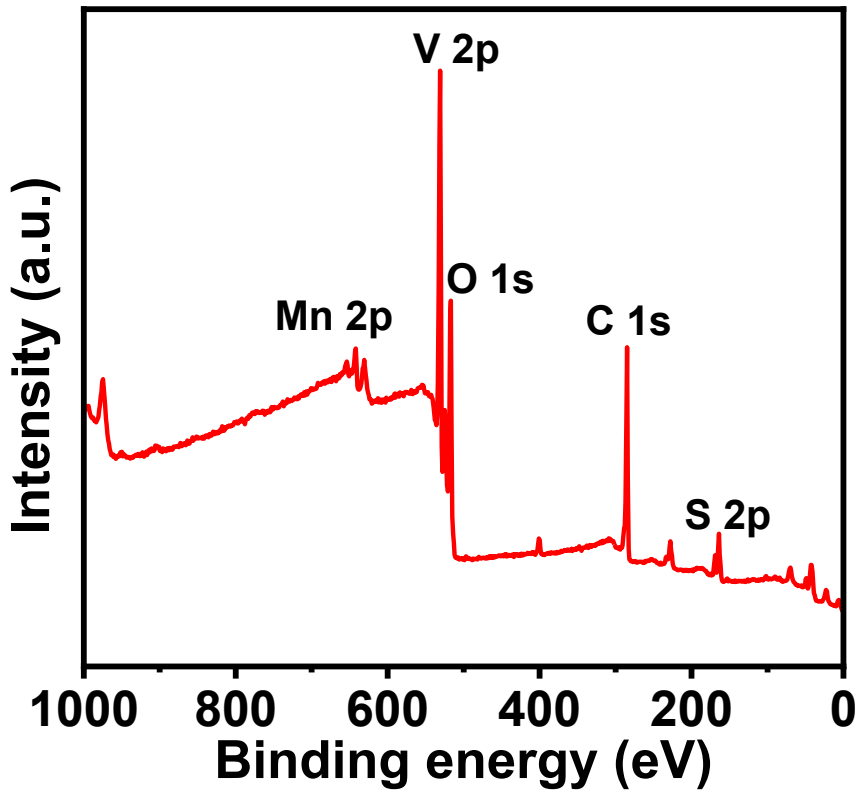

Supplementary Figure 5. XPS spectrum of Mn-VS_2.

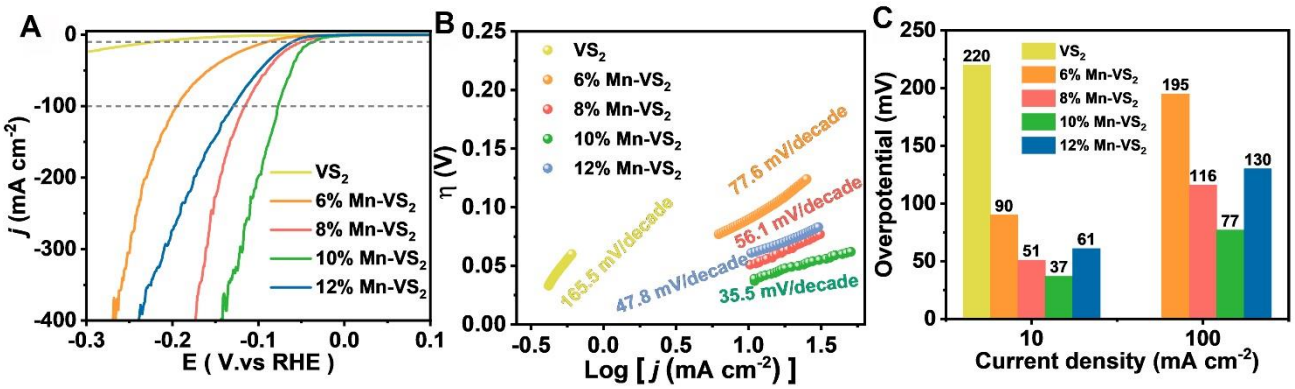

Supplementary Figure 6. Hydrogen evolution performance of VS_2 and Mn-VS_2 with varying doping levels was evaluated under iR compensation of 95%. Measurements were conducted in 0.5 M H_2SO_4. The findings include: (A) HER polarization curves demonstrating the electrocatalytic activity; (B) Tafel slopes depicting the kinetics of the hydrogen evolution reaction; (C) overpotentials required to achieve current densities of -10 mA cm^{-2} and -100 mA cm^{-2}.

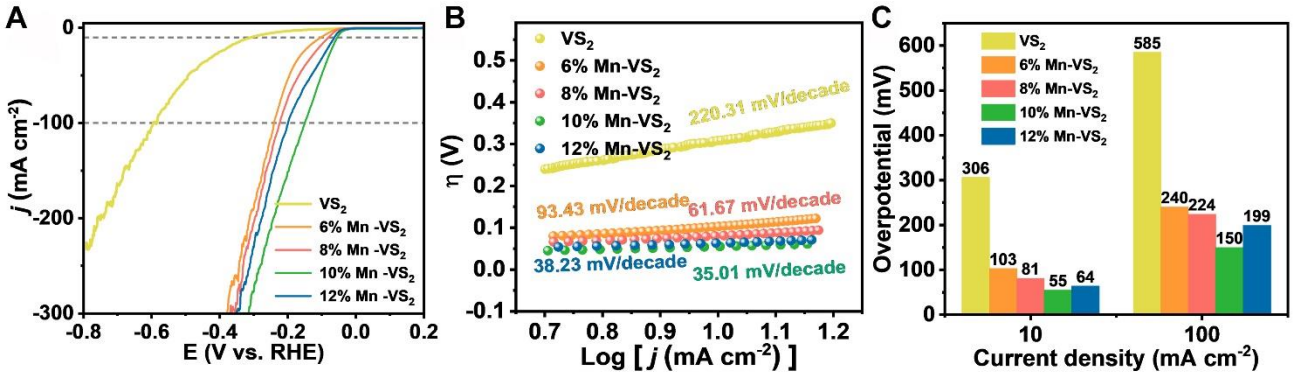

Supplementary Figure 7. Hydrogen evolution performance of VS_2 and Mn-VS_2 with varying doping levels was evaluated under iR compensation of 95%. Measurements were conducted in 1 M PBS. The findings include: (A) HER polarization curves demonstrating the electrocatalytic activity; (B) Tafel slopes depicting the kinetics of the hydrogen evolution reaction; (C) overpotentials required to achieve current densities of -10 $mA \cdot cm^{-2}$ and -100 $mA \cdot cm^{-2}$.

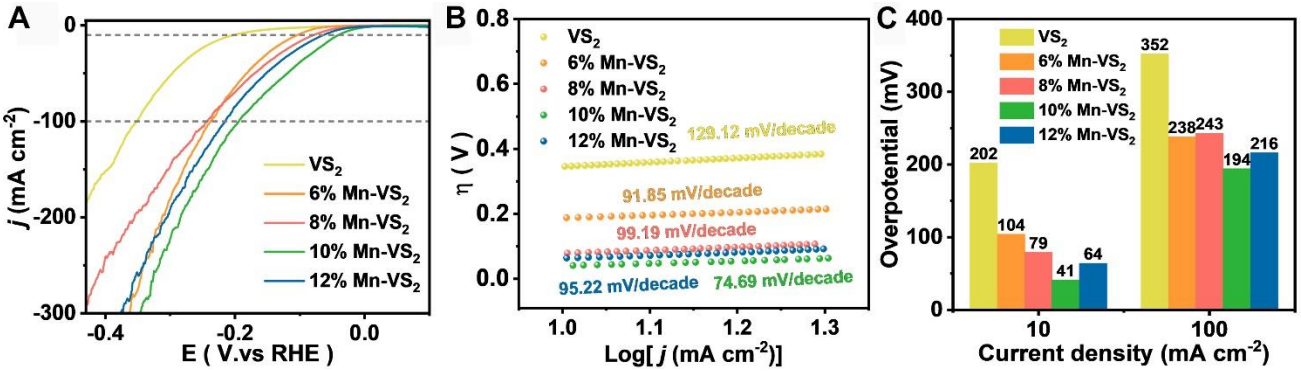

Supplementary Figure 8. Hydrogen evolution performance of VS_2 and Mn-VS_2 with varying doping levels was evaluated under iR compensation of 95%. Measurements were conducted in 1M KOH. The findings include: (A) HER polarization curves demonstrating the electrocatalytic activity; (B) Tafel slopes depicting the kinetics of the hydrogen evolution reaction; (C) overpotentials required to achieve current densities of -10 mA cm^{-2} and -100 mA cm^{-2}.

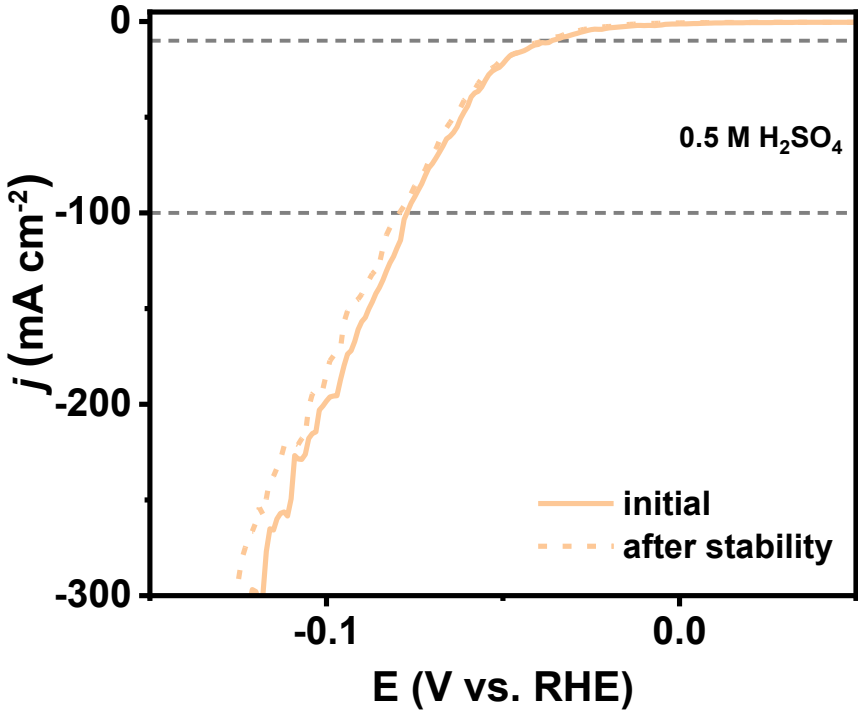

Supplementary Figure 9. LSV curves of Mn-VS_2 before and after running in 0.5 M H_2SO_4 for 100 h.

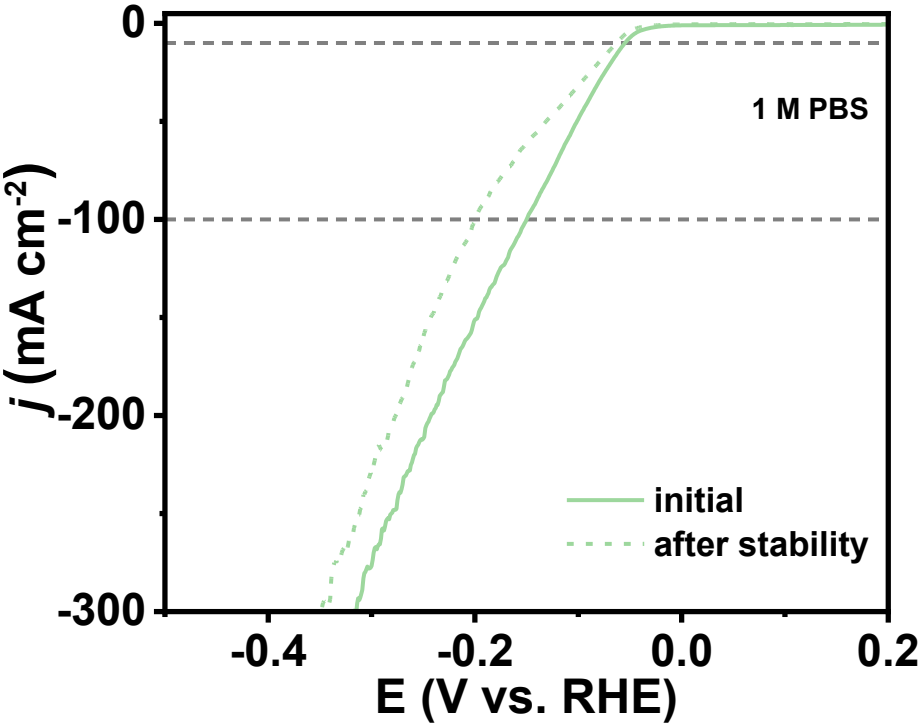

Supplementary Figure 10. LSV curves of Mn-VS_2 before and after running in 1 M PBS for 100 h.

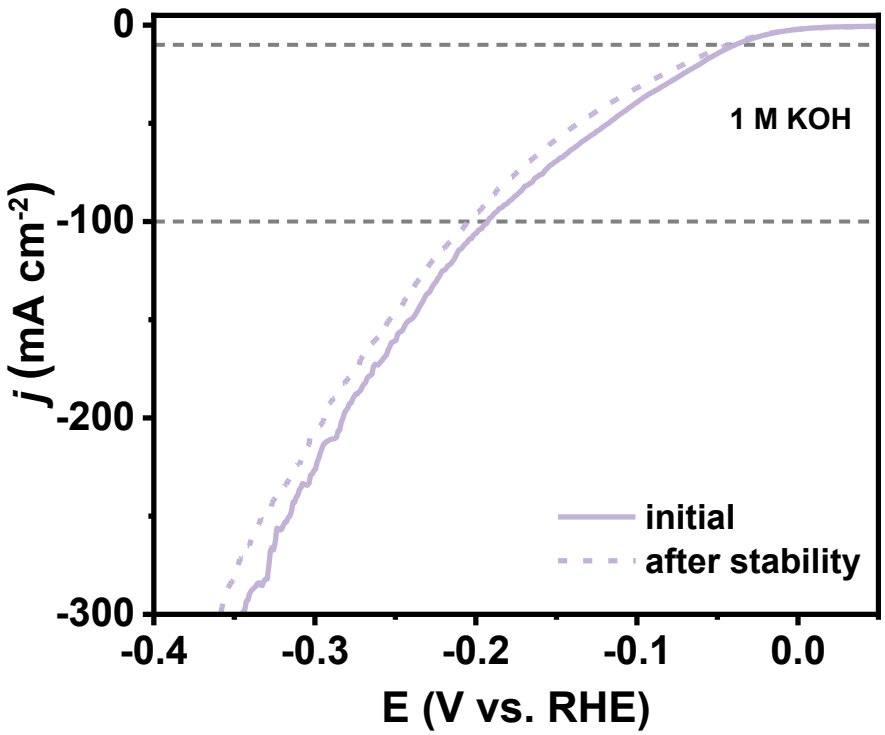

Supplementary Figure 11. LSV curves of Mn-VS_2 before and after running in 1 M KOH for 100 h.

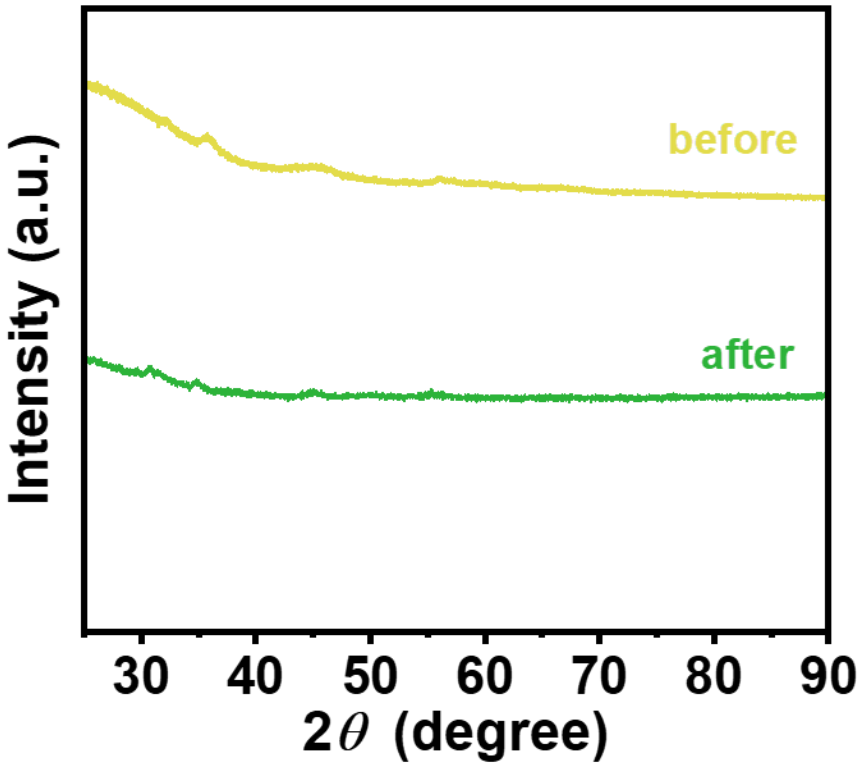

Supplementary Figure 12. XRD patterns of Mn-VS_2 before and after 100 h stability tests.

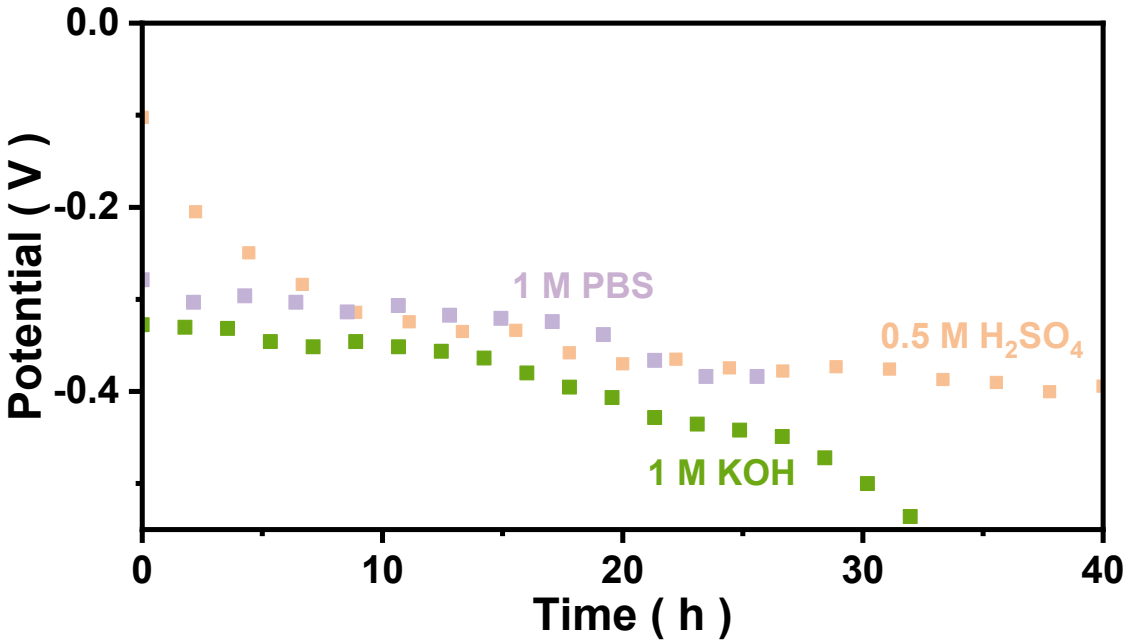

Supplementary Figure 13. The stability of VS_2 at a current density of -10 mA cm^{-2} in 0.5 M H_2SO_4, 1 M PBS, and 1 M KOH.

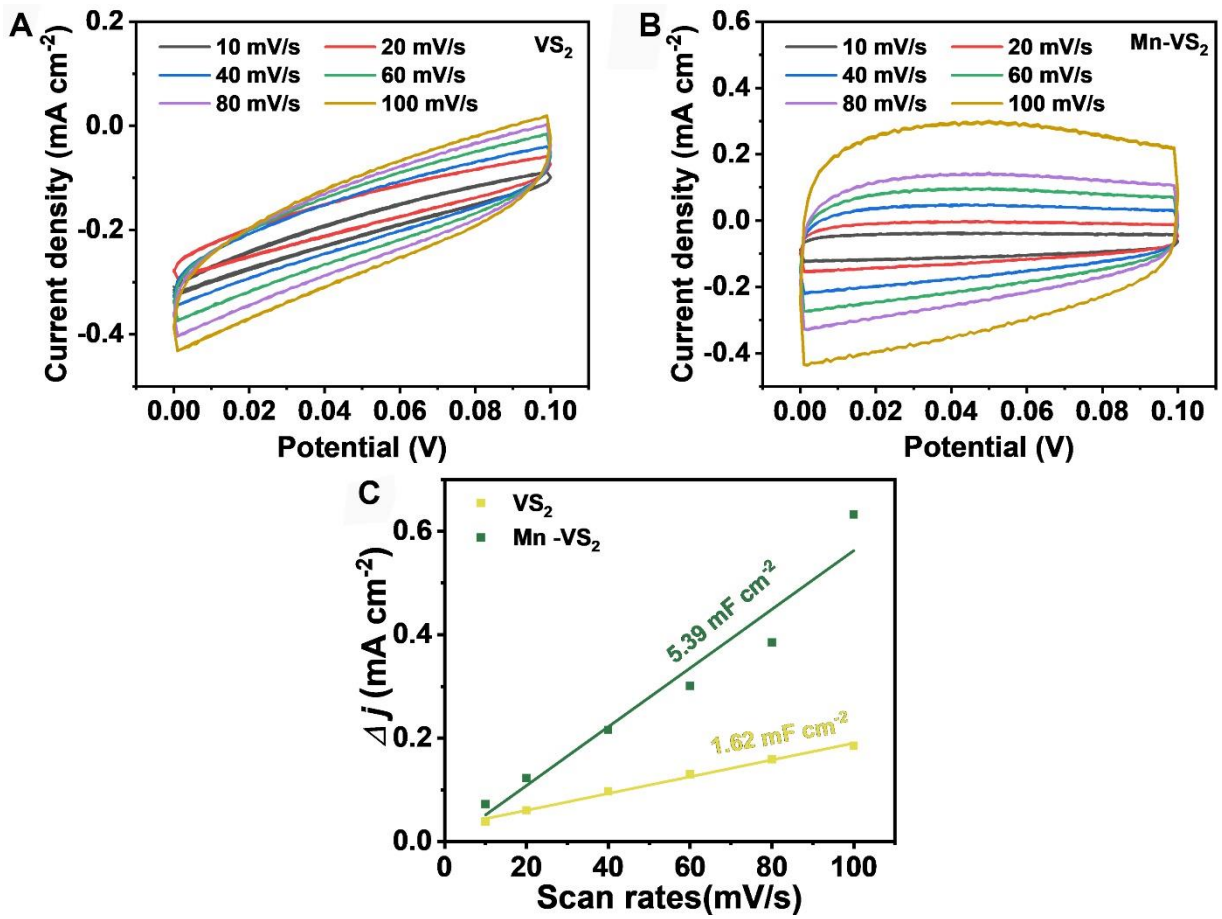

Supplementary Figure 14. (A and B) CV curves of Mn-VS_2 and VS_2 at different scan rates; (C) C_{dl} of VS_2 and Mn-VS_2.

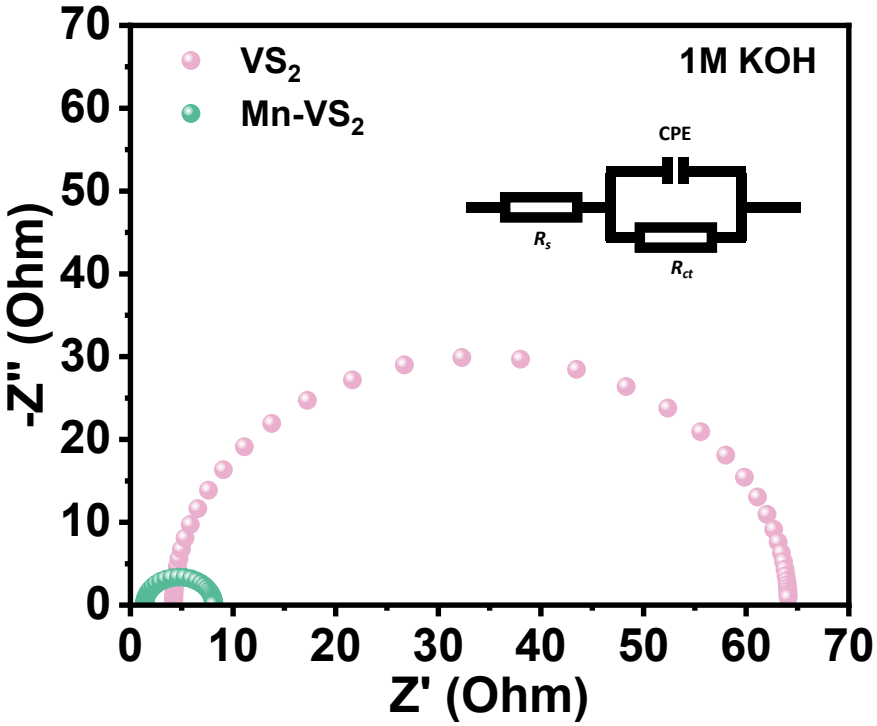

Supplementary Figure 15. Electrochemical impedance spectra of VS_2 and Mn-VS_2.

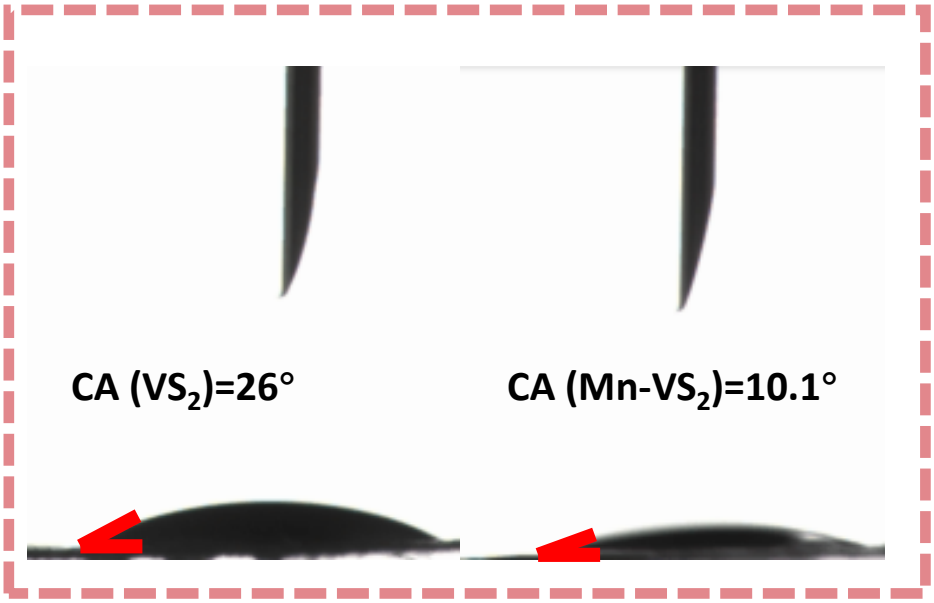

Supplementary Figure 16. Contact angle tests of VS_2 and Mn-VS_2 with deionized water.

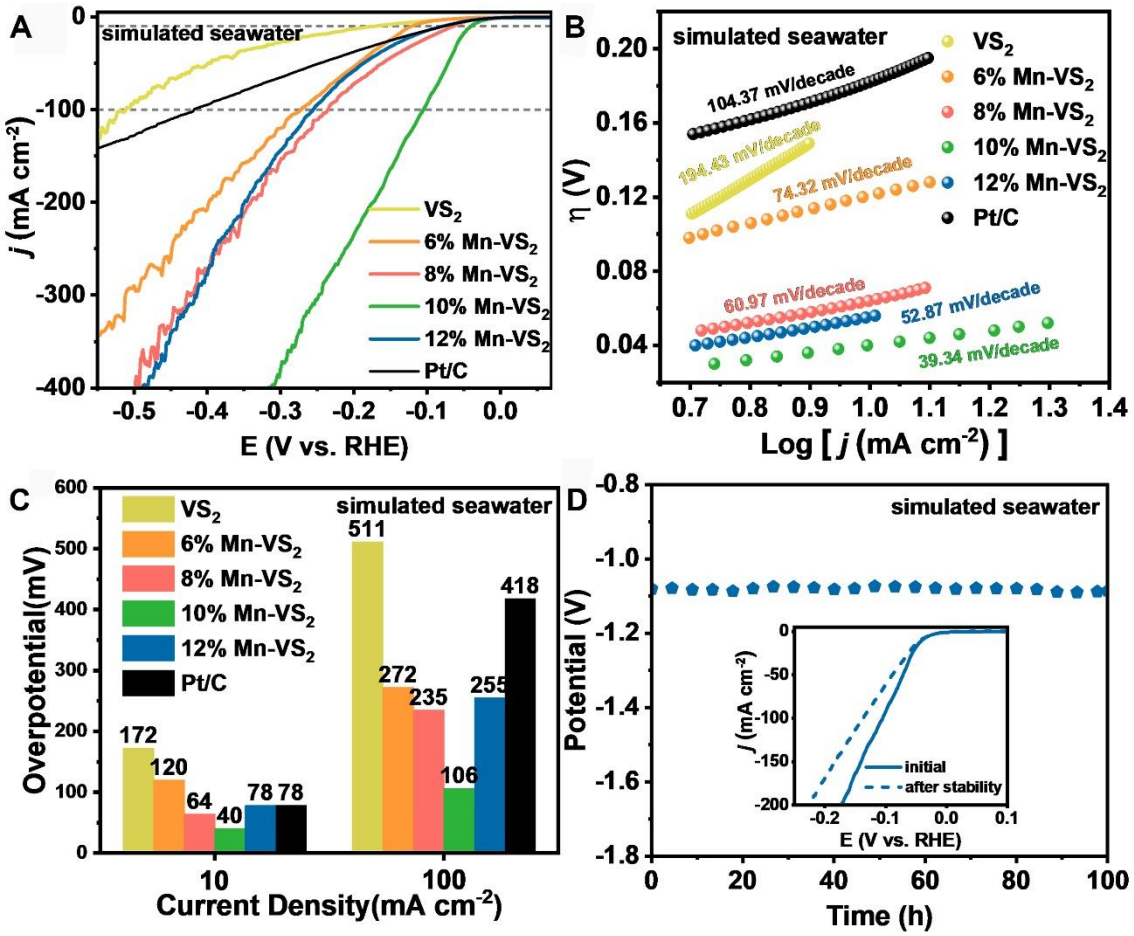

Supplementary Figure 17. Electrochemical performance analysis results of Pt/C, VS_2 and Mn-VS_2 with varying doping ratios in simulated seawater for HER application. (A) Polarization curves of Pt/C, VS_2 and Mn-VS_2 with different ratios; (B) Tafel slopes of Pt/C, VS_2 and Mn-VS_2 with varying ratios; (C) Overpotentials of Pt/C, VS_2 and Mn-VS_2 at current densities of -10 mA cm^{-2} and -100 mA·cm^{-2}; (D) Stability of Mn-VS_2 at a current density of 10 mA·cm^{-2}.

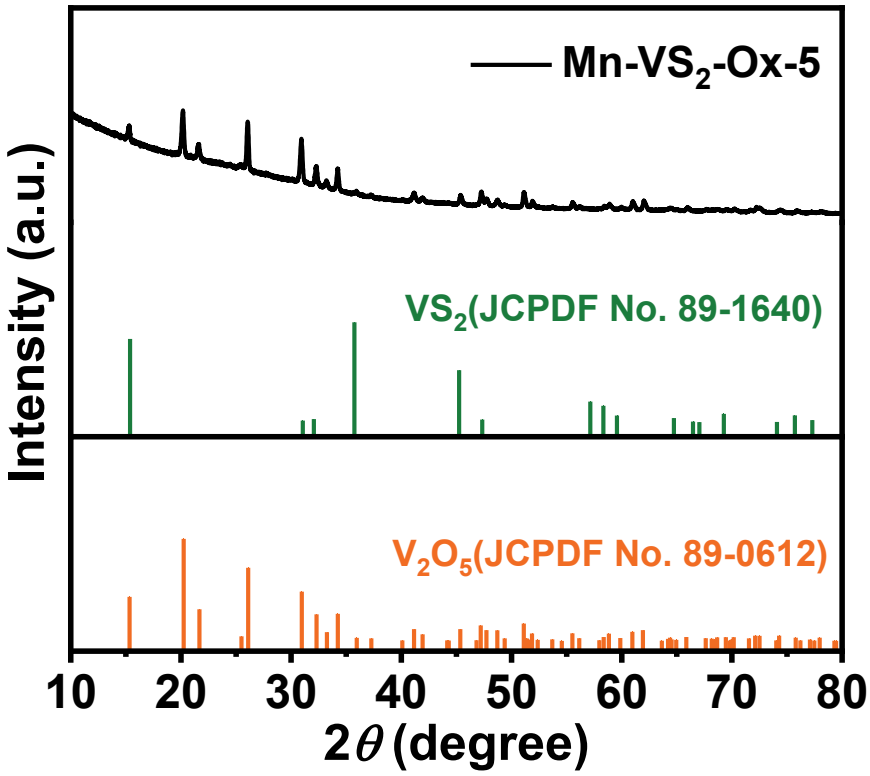

Supplementary Figure 18. XRD pattern of Mn-VS_2-Ox-5.

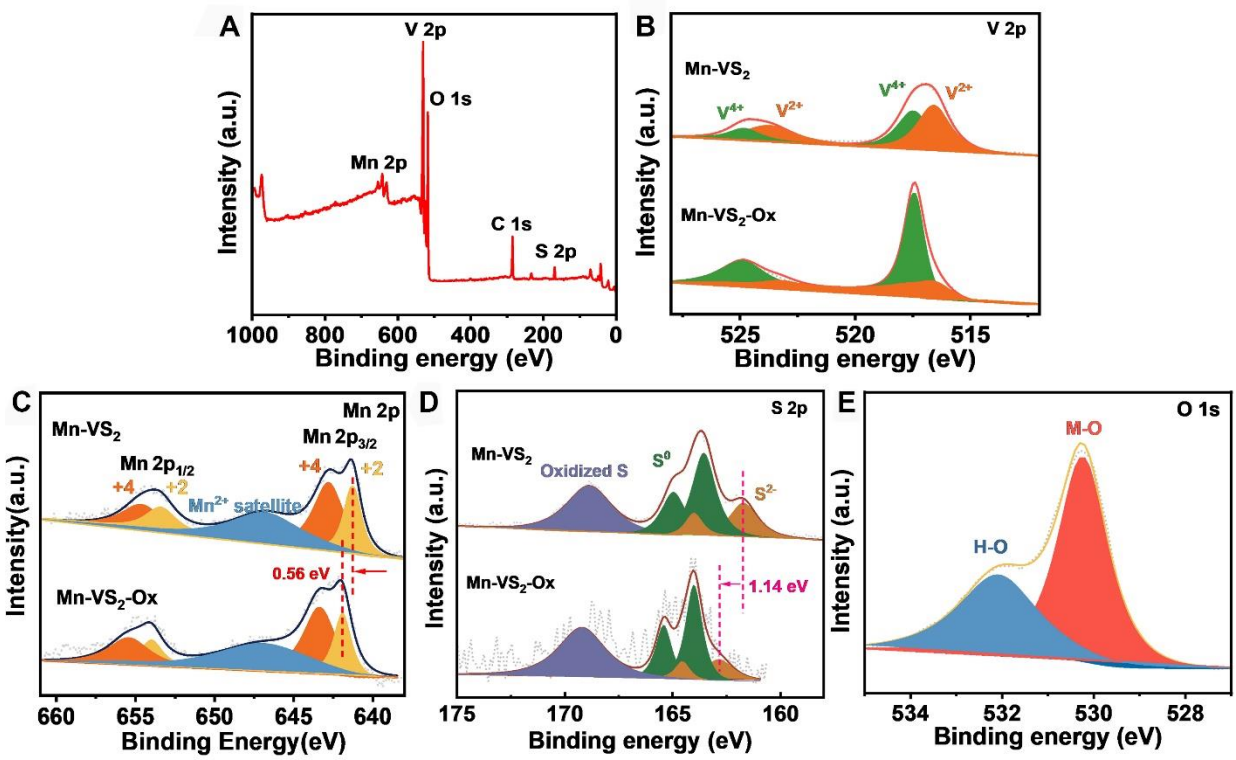

Supplementary Figure 19. (A) XPS spectrum of Mn-VS_2-Ox-5; (B) XPS spectra of V 2p; (C) Mn 2p (D) S 2p in Mn-VS_2 and Mn-VS_2-Ox-5; (E) XPS spectrum of O 1s in Mn-VS_2-Ox-5.

Supplementary Table 1. Comparison of HER performance between Mn-VS_2 and other transition metal sulfides

Catalyst	η (mV) at -10 $mA \cdot cm^{-2}$	Tafel slope ($mV \cdot dec^{-1}$)	Media	Ref.
Mn-VS_2	41 55 37	74.69 35.01 35.5	1 M KOH 1 M PBS 0.5 M H_2SO_4	This work
VS_2/MoS_2/MF	177	51	0.5 M H_2SO_4	[1]
Mo-VS_2	243	53	0.5 M H_2SO_4	[2]
Co-VS_2	234	93	0.5 M H_2SO_4	[3]
$NiCo_2S_4$@C_3N_4@VS_2	110	71.8	1 M KOH	[4]
N– Ni_3S_2/VS_2	151	107.5	1 M KOH	[5]
Co-VS_2/NF	164	52	1 M KOH	[6]
VS_2/MoS_2	115 148	33 69	0.5 M H_2SO_4 1 M KOH	[7]
1T-VSe_2	206	88	0.5 M H_2SO_4	[8]
1T-VSe_2	126	70	0.5 M H_2SO_4	[9]
Pt–MoS_2	60	96	0.1 M H_2SO_4	[10]
Co–WS_2	210	49	0.5 M H_2SO_4	[11]
Fe-WS_2	195	81	0.5 M H_2SO_4	[12]
$V_{0.8}Mo_{0.2}Se_2$	67.2 122.3 72.3	51 66 71	0.5 M H_2SO_4 1M PBS 1 M KOH	[13]
VN/Mo_2C	180	114	1M PBS	[14]
Ni_4Mo-V_2O_3	39.3	65.7	1M PBS	[15]
Ni_3N-VN	83	73	1M PBS	[16]

[1] Xu R, Huang J, Cao L, et al. VS_2 microflowers with in situ embedded few-layer MoS_2 nanobelts for enhanced hydrogen evolution reaction at high current density. Journal of The Electrochemical Society, 2020, 167(2): 026508.
[2] He W, Zheng X, Peng J, et al. Mo-dopant-strengthened basal-plane activity in VS_2 for accelerating hydrogen evolution reaction. Chemical Engineering Journal, 2020, 396: 125227.
[3] Zhao M, Yang M, Huang W, et al. Synergism on electronic structures and active edges of metallic vanadium disulfide nanosheets via Co doping for efficient hydrogen evolution reaction in seawater. ChemCatChem, 2021, 13(9): 2138-2144.
[4] Xu J, Zhu Y, Yu B, et al. Metallic 1T-VS_2 nanosheets featuring V^{2+} self-doping and mesopores towards an efficient hydrogen evolution reaction. Inorganic Chemistry Frontiers, 2019, 6(12): 3510-3517.
[5] Zhong X, Tang J, Wang J, et al. 3D heterostructured pure and N-doped Ni_3S_2/VS_2 nanosheets for high efficient overall water splitting. Electrochimica Acta, 2018, 269: 55-61.
[6] Feng T, Ouyang C, Zhan Z, et al. Cobalt doping VS_2 on nickel foam as a high efficient electrocatalyst for hydrogen evolution reaction. International Journal of Hydrogen Energy, 2022, 47(19): 10646-10653.
[7] Bolar S, Samanta P, Jang W, et al. Regulating the metal concentration for selective tuning of VS_2/MoS_2 heterostructures toward hydrogen evolution reaction in acidic and alkaline media. ACS Applied Energy Materials, 2022, 5(8): 10086-10097.
[8] Zhao W, Dong B, Guo Z, et al. Colloidal synthesis of VSe_2 single-layer nanosheets as novel electrocatalysts for the hydrogen evolution reaction. Chemical communications, 2016, 52(59): 9228-9231.
[9] Yan M, Pan X, Wang P, et al. Field-effect tuned adsorption dynamics of VSe_2 nanosheets for enhanced hydrogen evolution reaction. Nano Letters, 2017, 17(7): 4109-4115.
[10] Deng J, Li H, Xiao J, et al. Triggering the electrocatalytic hydrogen evolution activity of the inert two-dimensional MoS_2 surface via single-atom metal doping. Energy & Environmental Science, 2015, 8(5): 1594-1601.
[11] Shi X, Fields M, Park J, et al. Rapid flame doping of Co to WS_2 for efficient hydrogen evolution. Energy & Environmental Science, 2018, 11(8): 2270-2277.
[12] Kang M, Lin C, Yang H, et al. Proximity enhanced hydrogen evolution reactivity of substitutional doped monolayer WS_2. ACS Applied Materials & Interfaces, 2021, 13(16): 19406-19413.
[13] Zhang J, Li J, Huang H, et al. Spatial relation controllable di-defects synergy boosts electrocatalytic hydrogen evolution reaction over VSe_2 nanoflakes in all pH electrolytes. Small, 2022, 18(47): 2204557.
[14] Feng L, Li S, He D, et al. Heterostructured vn/Mo_2C nanoparticles as highly efficient pH-universal electrocatalysts toward the hydrogen evolution reaction. ACS Sustainable Chemistry & Engineering, 2021, 9(45): 15202-15211.
[15] Xie Z, Wang W, Ding D, et al. Accelerating hydrogen evolution at neutral pH by destabilization of water with a conducting oxophilic metal oxide. Journal of materials chemistry A, 2020, 8(24): 12169-12176.
[16] Ni Y, Ma X, Wang S, et al. Heterostructured nickel/vanadium nitrides composites for efficient electrocatalytic hydrogen evolution in neutral medium. Journal of Power Sources, 2022, 521: 230934.